AD-A110 095 NAVAL RESEARCH LAB WASHINGTON DC F/G 11/6
THICKNESS AND TEMPERATURE EFFECTS ON THE J-INTEGRAL COD RELATIO--ETC(U)
DEC 81 V PROVENZANO, C M GILMORE, F A SMIDT
UNCLASSIFIED NRL-MR-4696 NL

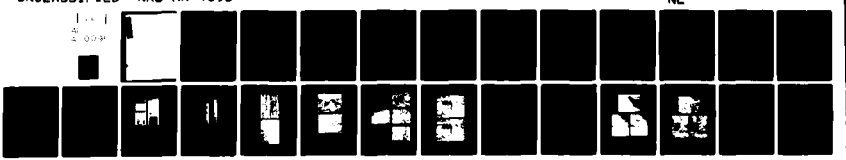

END
DATE FILMED
3 82
DTIC

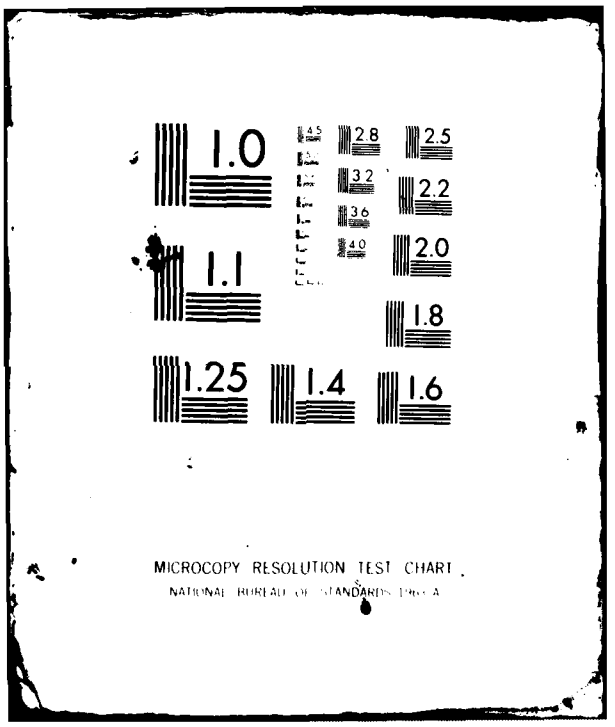
1.0
1.1
1.25
1.4
1.6
1.8
2.0
2.2
2.5
2.8
3.2
3.6
4.0
4.5
MICROCOPY RESOLUTION TEST CHART
NATIONAL BUREAU OF STANDARDS 1963-A

SECURITY CLASSIFICATION OF THIS PAGE (When Data Entered)

REPORT DOCUMENTATION PAGE		READ INSTRUCTIONS BEFORE COMPLETING FORM
1. REPORT NUMBER NRL Memorandum Report 4696	2. GOVT ACCESSION NO. AD-A110095	3. RECIPIENT'S CATALOG NUMBER
4. TITLE (and Subtitle) THICKNESS AND TEMPERATURE EFFECTS ON THE J-INTEGRAL COD RELATIONSHIP		5. TYPE OF REPORT & PERIOD COVERED Progress report on a continuing NRL problem. 6. PERFORMING ORG. REPORT NUMBER
7. AUTHOR(s) V. Provenzano, C. M. Gilmore,* F. A. Smidt, Jr., and J. R. Hawthorne		8. CONTRACT OR GRANT NUMBER(s)
9. PERFORMING ORGANIZATION NAME AND ADDRESS Naval Research Laboratory Washington, D.C. 20375		10. PROGRAM ELEMENT, PROJECT, TASK AREA & WORK UNIT NUMBERS 63-1314-0-2 RR022 11 41
11. CONTROLLING OFFICE NAME AND ADDRESS Office of Naval Research Arlington, VA		12. REPORT DATE December 31, 1981 13. NUMBER OF PAGES 26
14. MONITORING AGENCY NAME & ADDRESS(if different from Controlling Office)		15. SECURITY CLASS. (of this report) UNCLASSIFIED 15a. DECLASSIFICATION/DOWNGRADING SCHEDULE

16. DISTRIBUTION STATEMENT (of this Report)

Approved for public release; distribution unlimited.

17. DISTRIBUTION STATEMENT (of the abstract entered in Block 20, if different from Report)

18. SUPPLEMENTARY NOTES

*Also Department Chairman, Civil, Mechanical and Environmental Engineering, George Washington University, Washington, D.C. 20052.

19. KEY WORDS (Continue on reverse side if necessary and identify by block number)

Alloy HT-9	J-Integral
Crack opening displacement (COD)	Scanning electron microscopy (SEM)
Fractography	Stereography
Fracture toughness	Stretched zone

20. ABSTRACT (Continue on reverse side if necessary and identify by block number)

The fracture surfaces of compact tension (CT) specimens of HT-9 martensitic stainless steel previously tested at room temperature and at 200°C have been examined by scanning electron microscopy (SEM) to characterize the failure processes and establish correlations with fracture toughness properties; the fracture toughness of HT-9 for two specimen thicknesses (2.5 and 12.7 mm) was determined by conducting J-integral tests using the single specimen unloading compliance method. The microstructure of the specimens was also quantitatively characterized by

(Abstract continued)

DD FORM 1 JAN 73 1473 EDITION OF 1 NOV 65 IS OBSOLETE
S/N 0102-014-6601

SECURITY CLASSIFICATION OF THIS PAGE (When Data Entered)

20. ABSTRACT (Continued)

stereographic techniques. For the 12.7 mm specimens a good correlation was found between the height of the stretched zone and J_{Ic}, and a constraint factor of about 2.0 was observed. For the 2.5 mm specimen the stretched zone was not well defined and an unrealistic constraint factor of 6 was observed. The 2.5 mm specimens resulted in higher values of the J_{Ic} and lower temperature dependence than the 12.7 mm specimens. The results indicate that thin specimens that do not satisfy the validity criterion proposed by the ASTM E24 committee may fail by mechanisms that are different than the failure mechanism in thicker specimens.

CONTENTS

THICKNESS AND TEMPERATURE EFFECTS ON THE J-INTEGRAL COD RELATIONSHIP

INTRODUCTION

Fracture mechanics has been successful in providing a rational framework for the description of the fracture process and the design of engineering components using a continuum model for the structure. Experience and observation tell us that microstructural features of the material influence its fracture behavior and ultimately determine the level of toughness. This work is part of a larger effort to integrate the macroscopic and microscopic approaches to fracture so as to provide a better understanding of the role of microstructure and the optimization of toughness through microstructural control. The present investigation of the influence of thickness and temperature on the J integral-Crack Opening Displacement relationship is particularly pertinent to the development of test specimens for characterization of materials to be used in advanced nuclear systems where the volume of space available for irradiation of specimens precludes the use of standard size specimens.

When a load is applied to a material containing a crack, the crack faces are opened or displaced causing a crack opening displacement (COD). It was suggested by Wells [1] that the magnitude of the COD at fracture (δc) was a measure of the materials resistance to fracture. Wells developed a relationship between $\mathcal{J}_c$, the fracture toughness, and the critical value of the COD at fracture for plane stress conditions. This relationship is given by:

$$\mathcal{J}_c = \frac{\pi}{4} \sigma_y \delta_c, \tag{1}$$

where σ_y is the yield stress.

Burdekin and Stone [2] utilized Dugdale's [3] model for COD in thin sheets to develop the relationship:

$$\mathcal{J}_c = \sigma_y \delta_c \tag{2}$$

Broek [4] utilized an equation of the type:

$$\mathcal{J}_c = m \sigma_y \delta_c \tag{3}$$

where m was a parameter dependent upon the amount of plastic constraint. For a plane strain condition with maximum constraint, m was taken to be 3, and for plane stress with a minimum of constraint m was taken to be 1.33.

To treat elastic-plastic fracture problems the concept of the J integral was developed by Rice [5]. For elastic fracture it was shown that:

$$J_{Ic} = \mathcal{J}_c \tag{4}$$

In addition, Begley and Landes [6] observed that the value of J_{Ic} from an elastic-

Manuscript submitted October 19, 1981.

plastic test was equal to J_{Ic} from an elastic test:

$$J_{Ic}\,(\text{plastic}) = J_{Ic}\,(\text{elastic}). \tag{5}$$

The interest in J_{Ic} resulted from the possibility of being able to treat elastic-plastic fracture problems and to test thinner specimens than required to determine the plane strain critical stress intensity.

Combining equations (3) and (5) results in

$$J_{Ic} = m\,\sigma_y\,\delta_c. \tag{6}$$

For work hardening materials, Knott [7] has used the equation:

$$J_{Ic} = m\,\sigma_f\,\delta_c \tag{7}$$

where flow stress (σ_f) was taken to be the average of the yield and ultimate strengths. From Eqs. (1), (2), and (3) the values of m could range from 0.79 to 3. The higher values of m correspond to higher values of constraint as observed in plane strain fracture; the lower values of m correspond to lower constraint as in plane stress fracture.

Kobayashi [8] proposed that the critical stretched zone width $(SZW)_c$ was related to J_{Ic} through the equation:

$$(SZW)_c = \frac{CJ_{Ic}}{E} \tag{8}$$

where E was Young's elastic modulus and C was a constant. The stretched zone width was related to the COD through the relationship:

$$\text{COD} = (1.1 \text{ to } 1.4)\,\text{SZW}. \tag{9}$$

With the use of Eq. 9, the Eq. 8 proposed by Kobayashi is essentially the same as Eq. 7 except that a correction for elastic modulus can be made. Kobayashi observed very little variation in $(SZW)_c$ with changes in specimen thickness and changes in material.

A number of techniques and approximations have been employed to measure the magnitude of the COD. For example, Burdekin and Stone [2] utilized a paddle wheel COD meter, and Fields and Miller [9] made use of a silicone rubber to infiltrate cracks under load. Several authors have utilized fracture surface features as an indication of the COD. Rice and Johnson [10] developed a model for fracture by ductile void growth at the crack tip where the crack opening displacement (COD) was related to the mean particle spacing in a planar section and to the initial void size. Broek [4] equated the crack opening displacement to the size of the stretched zone that was measured with large angle stereo pairs produced from transmission electron micrographs of a surface replica. Broek found that m averaged about 2.5 for a group of 14 aluminum alloy specimens.

In this work the relationship between the fracture surface microstructure and the value of the J integral in HT-9 alloy steel was studied. Following Landes and McCabe [11], the fracture process in a test has been divided into four steps as is shown in Fig. 1.

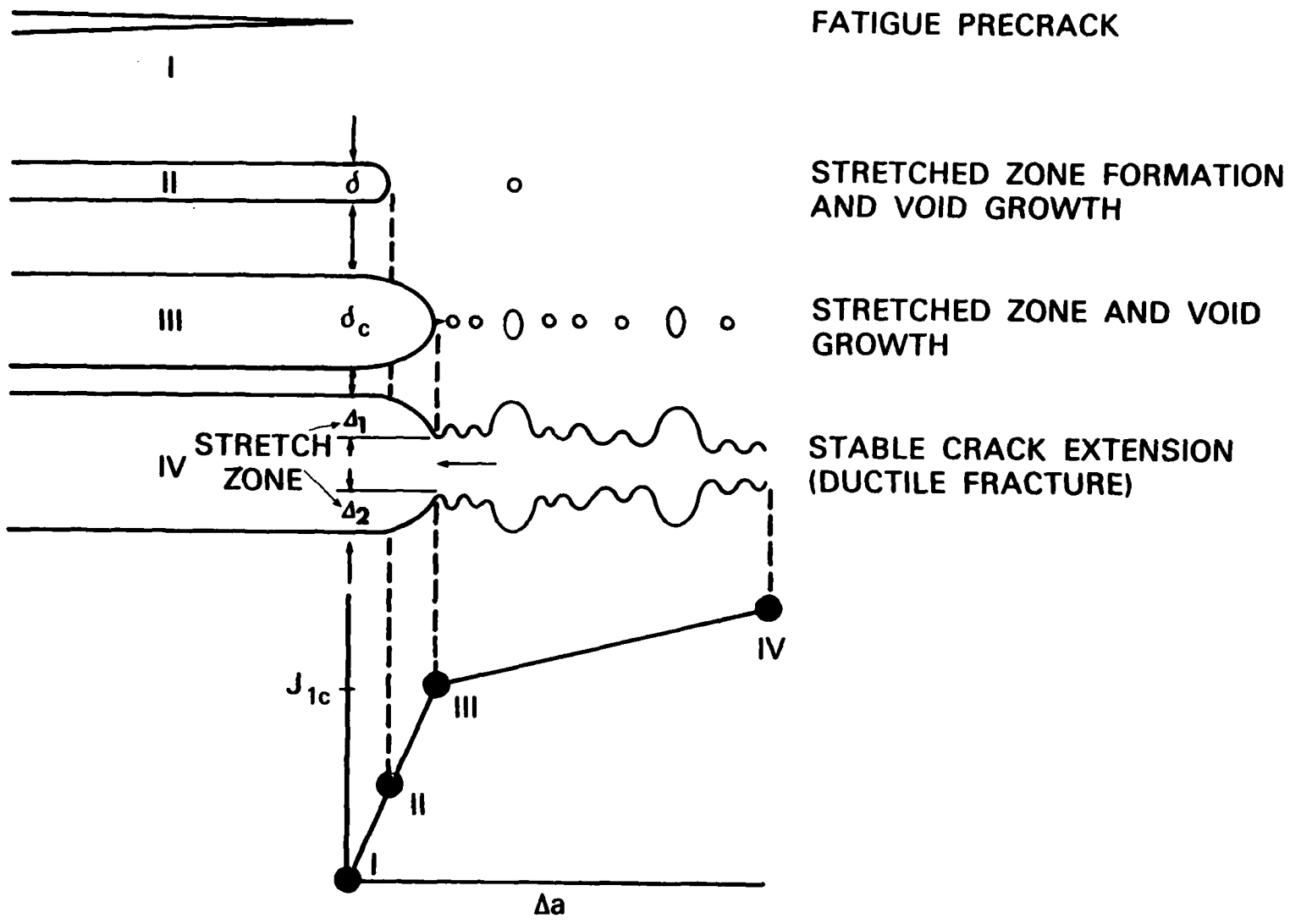

Fig. 1 — A schematic model of crack propagation in fracture toughness specimens together with the corresponding regime in J-R curve. The magnitude of the crack opening displacement (COD) at fracture (δ_c) is equal to the sum of Δ_1 and Δ_2.

1. Blunting of the pre-existing crack tip - The blunting of the crack tip occurs by stretching of the metal through plastic deformation at the crack tip. The fatigue precrack can be assumed to be atomically sharp thus the step that occurs at the stretched zone is totally due to deformation during fracture.

2. Initiation of stable crack growth from the blunted crack tip - The initiation of crack growth should correspond to the instant where the value of the J integral is equal to J_{Ic}.

3. Stable crack growth by plastic deformation mechanisms - The primary mechanism of stable crack growth is microvoid coalesence.

4. Instability due to rapid crack propagation - Loss [12] has observed that in A533-B bainitic steel instability occurs when the fracture mode changes from a ductile void coalescence to cleavage fracture.

EXPERIMENTAL PROCEDURE

In the present study, two sets of Alloy HT-9 were tested. Each set consisted of two specimens; one set was 2.5 mm thick (Type 0.1T-CT) and the other set was 12.7 mm thick (Type 0.5T-CT). All four specimens were cut from a commercially heat treated, 35-mm diam rod (NRL stock, heat 91354). Two compact tension (CT) specimens of each thickness were used to evaluate the static fracture toughness of the HT-9 rod at 24 and 200°C. Figures 2 and 3 show the CT specimen design and the specimen orientation in the 33-mm diam rod.

The fracture toughness of the rod was measured by conducting J-integral tests. The J-R curves for the fracture toughness tests were obtained by means of the single specimen compliance (SSC) technique. Additional details on the test method are given in Refs. 12 and 13. Prior to the J-integral tests, the specimens were fatigue precracked to about 1.78 mm crack length in order to obtain a sharp crack. The 12.7 mm thick specimens were 20 percent side grooved to aid crack front straightness.

Fractographic examinations on the failed specimens were performed on a Coates and Welter 106A field emission scanning electron microscope (SEM). Specimen tilt of five degrees was found to be optimum for strereoscopic examinations and quantitative measurements of void depth and stretched zone size. The stereographic measurements were performed by employing a semi-automatic visual analysis system that incorporates a Hewlett-Packard Model 9830A mini-computer for data recording and reduction. A schematic diagram of the system is shown in Fig. 4. More details about the system may be found in Refs. 14 and 15.

The size of the stretched zone in each specimen was determined stereographically by making several measurements along the crack front and then taking an average of these measurements. Multiple measurements of the same crack profiles yielded a standard deviation of 7 percent. The stretched zone was defined as the featureless region bounded by the fatigue precrack on one side and the stable crack extension on the other. Typically, the stable crack extension was characterized by microvoid coalescence (dimpled rupture) which makes it easy to distinguish it from the stretched zone. The stretched zone size was checked for consistency by making measurements on both halves of a specimen. Stereographic measurements were also conducted to obtain the depth of large voids in the specimen fracture surface.

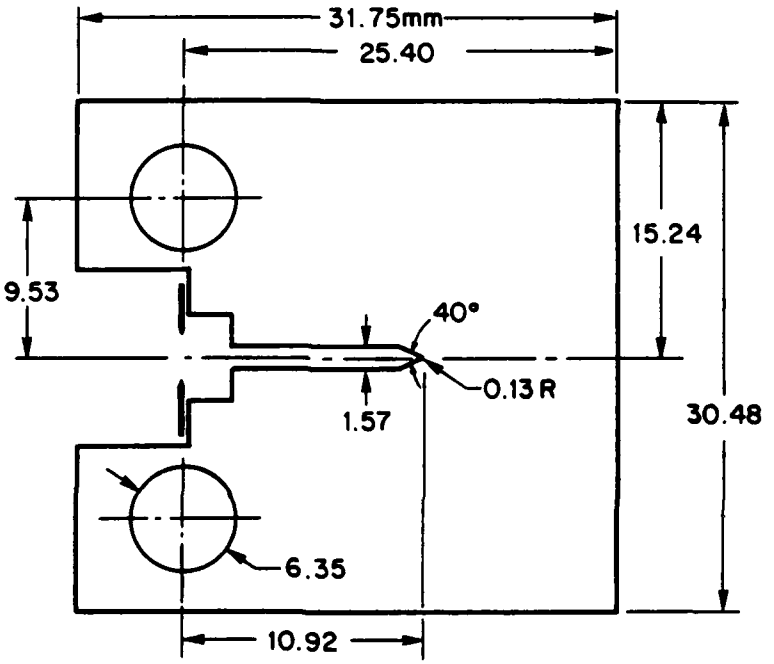

Fig. 2 — 0.1T-CT and 0.5T-CT specimen design. A fatigue precrack of 1.78 mm is added prior to testing.

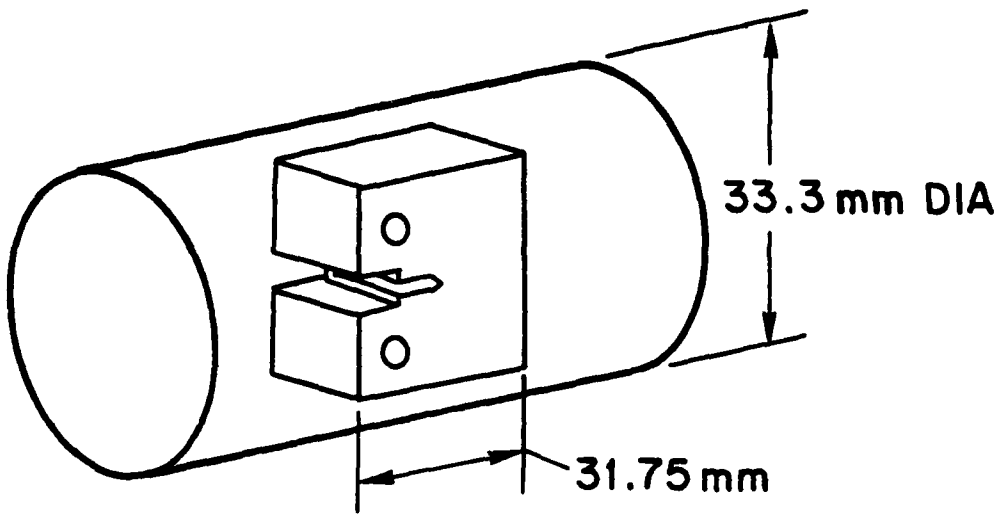

Fig. 3 — Specimen orientation in test stock (33-mm rod).

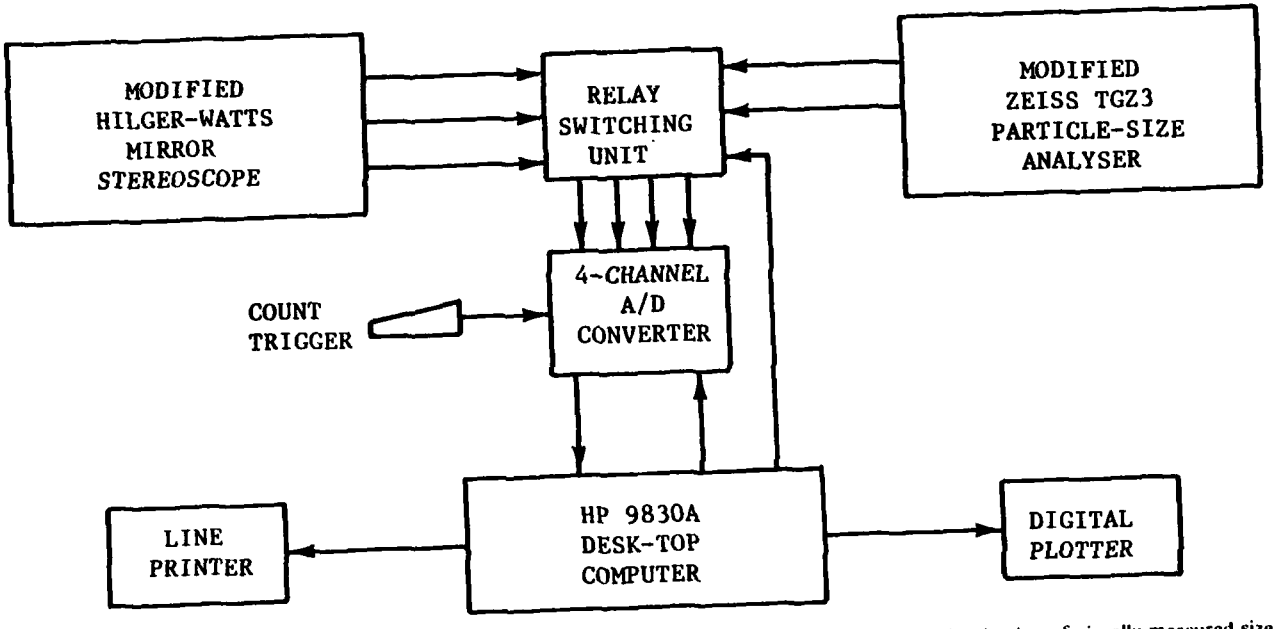

Fig. 4 — Semi-automatic visual micrograph analysis system incorporating computer aided recording and reduction of visually measured size and stereo position data.

EXPERIMENTAL RESULTS

The J-R curves for the specimens are presented in Figs. 5 and 6. As can be seen from Fig. 5, the 0.5T specimens show a higher static fracture toughness at 200°C than at 24°C. The thinner specimens (0.1T) show less difference in fracture toughness at the two test temperatures (Fig. 6). The fracture toughness of both 0.1T specimens was higher than either of the 0.5T specimens.

The optical micrographs of the fracture surfaces, shown in Figs. 7 and 8, indicate that conditions approximating plane strain were present in the 12.7 mm thick specimens, while conditions approximating plane stress were present in the 2.5 mm thick specimens.

The two SEM fractographs presented in Fig. 9 are from the 12.7 mm thick specimens tested at 24°C (left) and 200°C (right). The SEM micrographs show that for both test conditions the crack front was fairly straight and well defined. The crack extension, shown in the upper part of both fractographs was preceded by a stretch zone (SZ). Secondary cracking at the stretched zone next to the end of the precrack was present in both surfaces. The secondary cracking was roughly parallel to the primary crack front and approximately at 45 degrees to the plane of fracture. Figure 10 shows two higher magnification SEM micrographs of the fracture surfaces of the 12.7 mm specimens in the stable crack extension region. The overall fracture mode for the specimens was ductile rupture (microvoid coalescence) characterized by areas of large and small voids. The voids appeared to have nucleated around precipitate particles or inclusions and expanded as the region ahead of the crack deformed. Crack propagation appeared to occur when the larger voids linked together with the crack tip by the formation of small voids. The ductile failure observed in both specimens was consistent with the Charpy-V notch ductility curve obtained on this same HT-9 material [16]. The 24°C temperature was in the upper part of the transition region of the Charpy-V notch curve while 200°C resided in the upper shelf energy region.

The SEM fractographs shown in Fig. 11 are of the 12.7 mm thick specimen tested at 24°C. The lower magnification micrograph on the left-hand side of the figure shows the precrack area, the stretched zone, and the stable crack extension region. The higher magnification micrographs shown on the right-hand side of the figure provide more details at the three different fracture regions. The precrack area (panel d) was characterized by fracture features normally associated with low stress fatigue, the stretched zone (panel c) was featureless while the crack extension region, as previously observed in Fig. 10, was characterized by dimple rupture (panel b).

The stretched zone boundaries were first determined by high magnification micrographs. Figure 12 shows a typical SEM stereo pair used to measure the size of the stretched zone. Figure 13 is an example of a fracture profile obtained using the two SEM micrographs shown in Fig. 12. From fracture profiles such as this the SZ size was determined by measuring the height of the smooth featureless region relative to the fatigue precrack.

An attempt was made on the 12.7 mm thick specimens to correlate the average depth of the large voids present in the crack extension region (Figs. 10 and 11) next to the stretched zone to J_{Ic}. As in the case of SZ size, the void depth was measured stereographically. It was found that the void depth had a large scatter, and when the results on the void depths were substituted in Eq. 7, they yielded a value of m close to 1. An m value of 1 indicates plane stress conditions, while the optical macrographs in Fig. 7 show instead that conditions of plane strain were present.

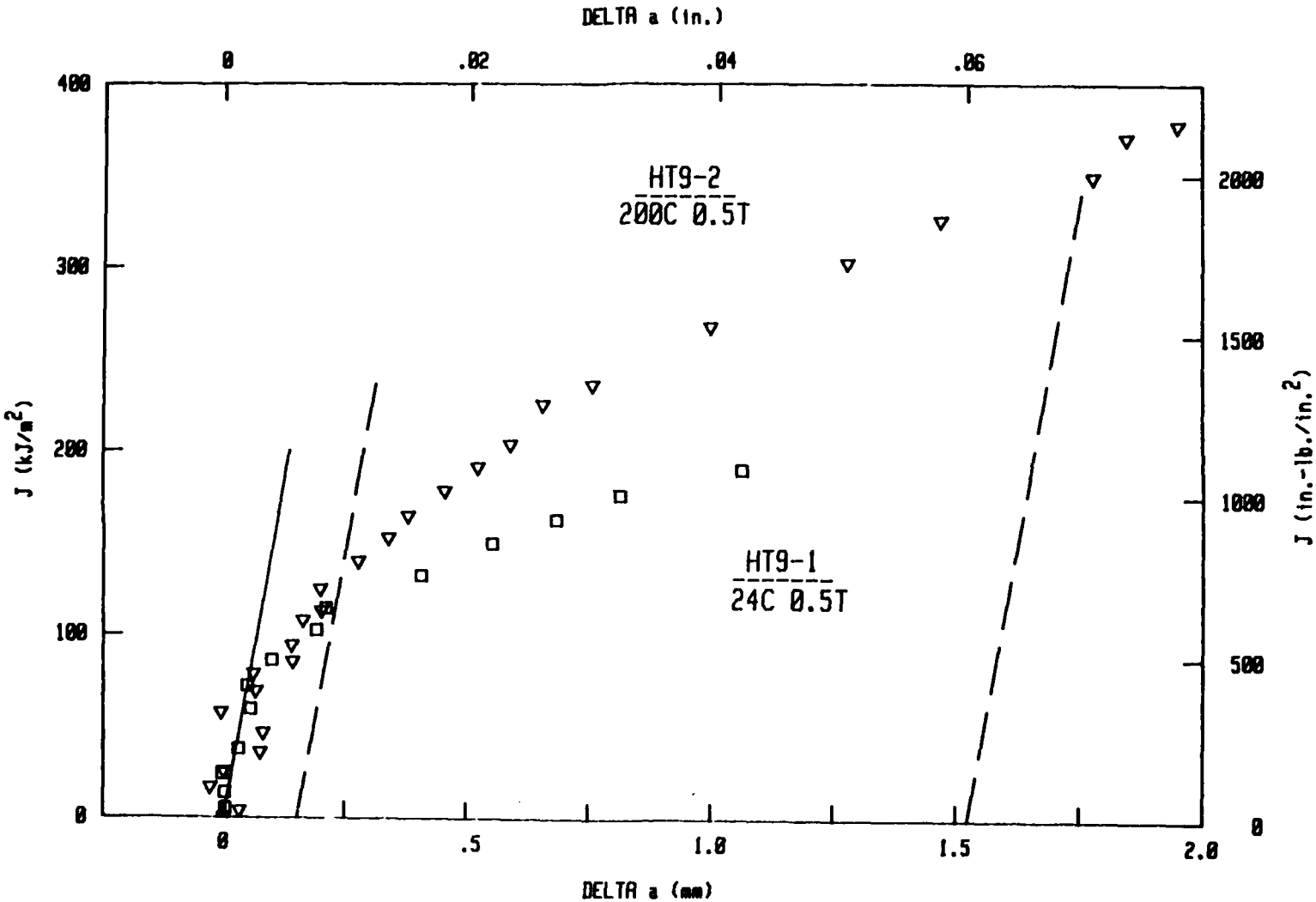

Fig. 5 — J-R curves for Alloy HT-9, Heat 91354, at 24 and 200°C developed with 20 percent side grooved 0.5T-CT specimens.

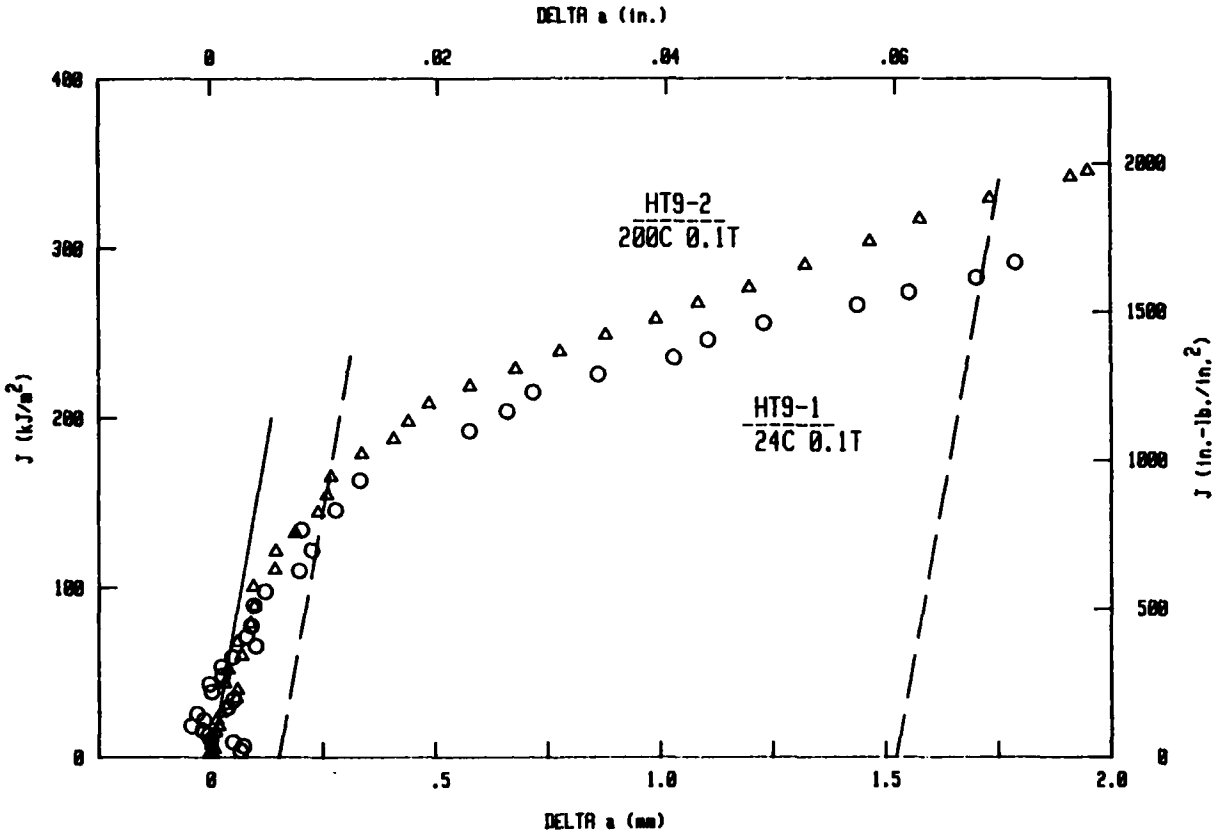

Fig. 6 — J-R curves for Alloy HT-9, Heat 91354, at 24 and 200 °C developed with zero percent side grooved 0.1T-CT specimens.

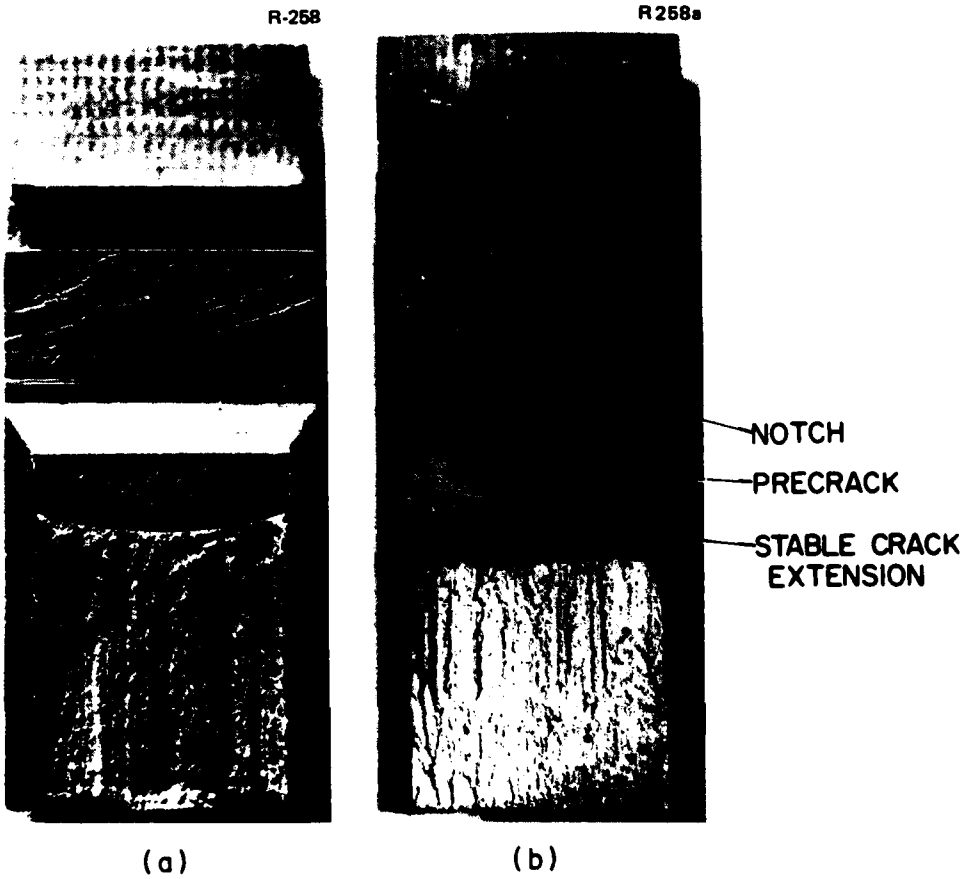

Fig. 7 — Fracture surfaces of 0.5T-CT specimens of Alloy HT-9 Heat 91354, tested at (a) 24 and (b) 200°C. The region of stable crack extension at 200°C was revealed by post-test heat treatment.

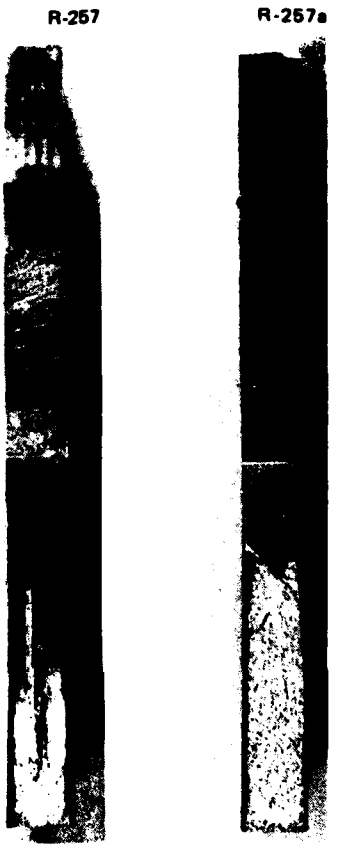

Fig. 8 — Fracture surfaces of 0.1T-CT specimen of Alloy HT-9, Hat 91354, tested at (a) 24 and (b) 200°C. The thickness contractions and slant fracture are evidence of plane stress conditions.

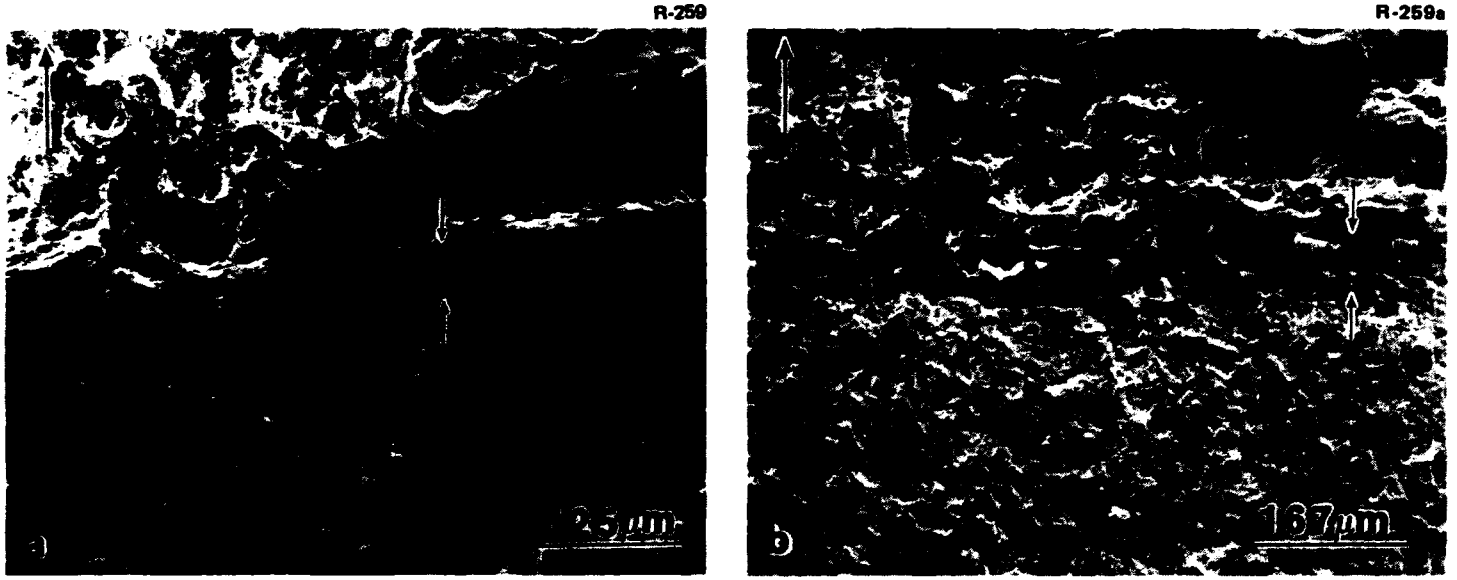

Fig. 9 — Fracture surface (SEM) of 0.5T-CT specimens of Alloy HT-9, Heat 91354, tested at (a) 24 and (b) 200°C. Arrows show direction of macroscopic crack propagation. Both micrographs show the precrack region, the stretched zone, and the region of stable crack extension. The approximate width of the stretched zone is indicated by the smaller arrows on the micrographs.

R-256

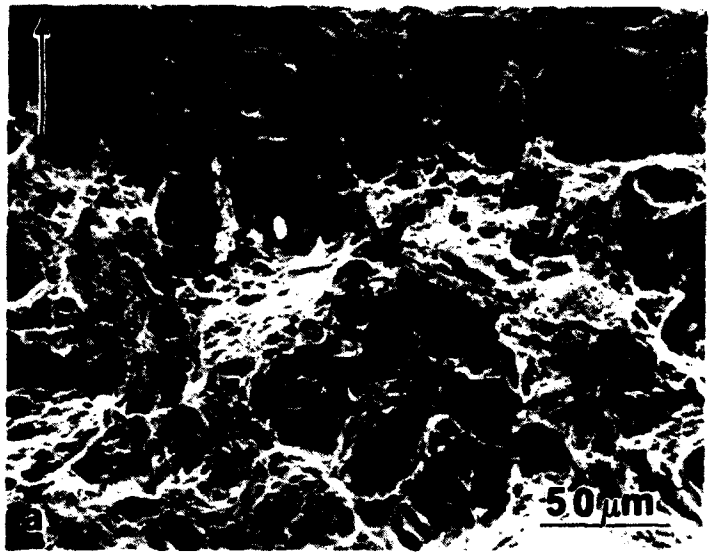

R-256a

Fig. 10 — Fracture surfaces (SEM) of 0.5T-CT specimens of Alloy HT-9, Heat 91354, tested at (a) 24 and (b) 200°C. Arrows show direction of macroscopic crack propagation. The micrographs show that the region of stable crack extension in both specimens is characterized by ductile fracture with large and small voids nucleating at precipitate and inclusion particles.

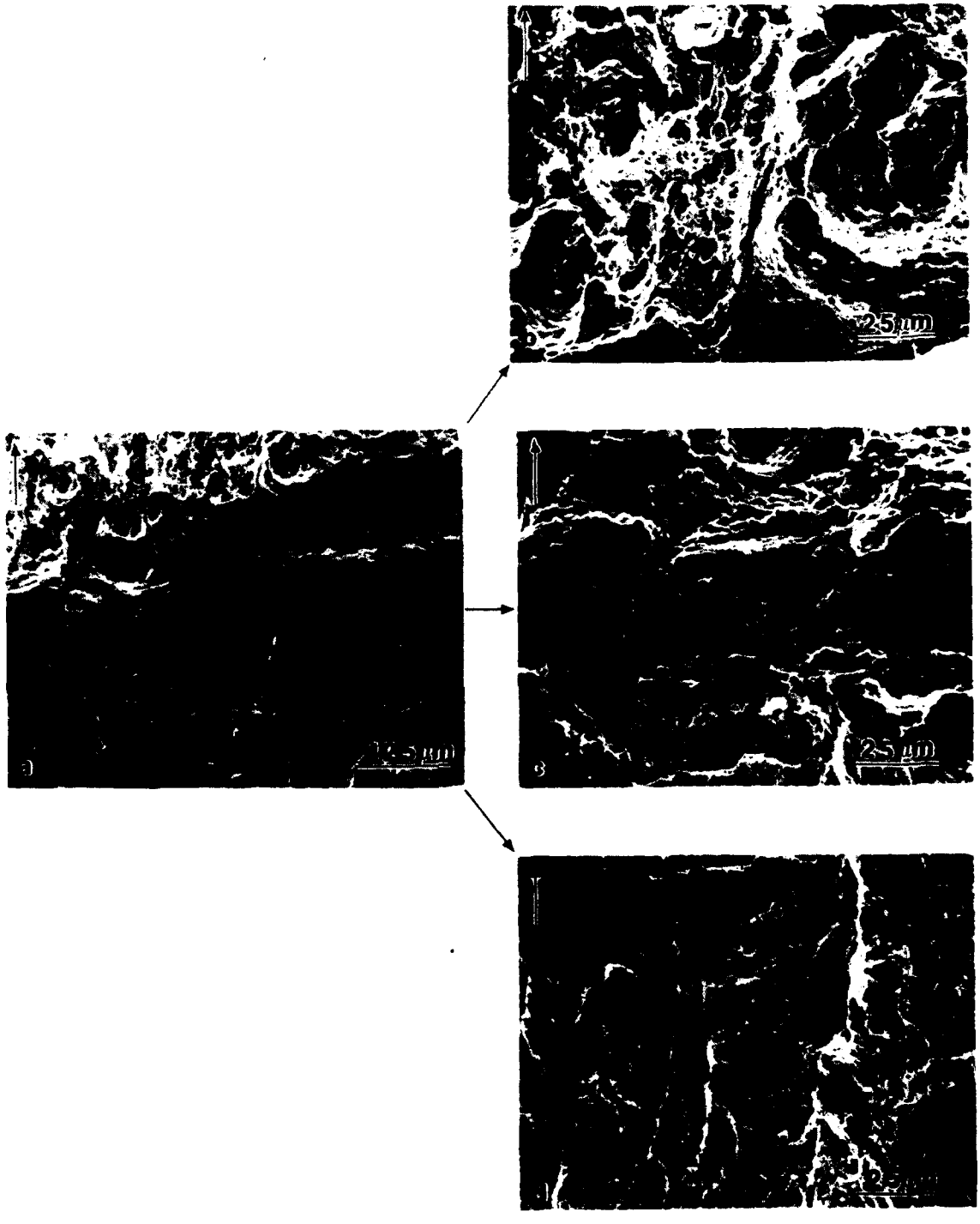

Fig. 11 — Fracture surfaces (SEM) of 0.5T-CT specimen of Alloy HT-9, Heat 91354, tested at 24°C. Arrows show direction of macroscopic crack propagation. The higher magnification micrographs on the right of the figure show fractographic features of precrack region (panel d), stretched zone (panel c), and stable crack extension region (panel b).

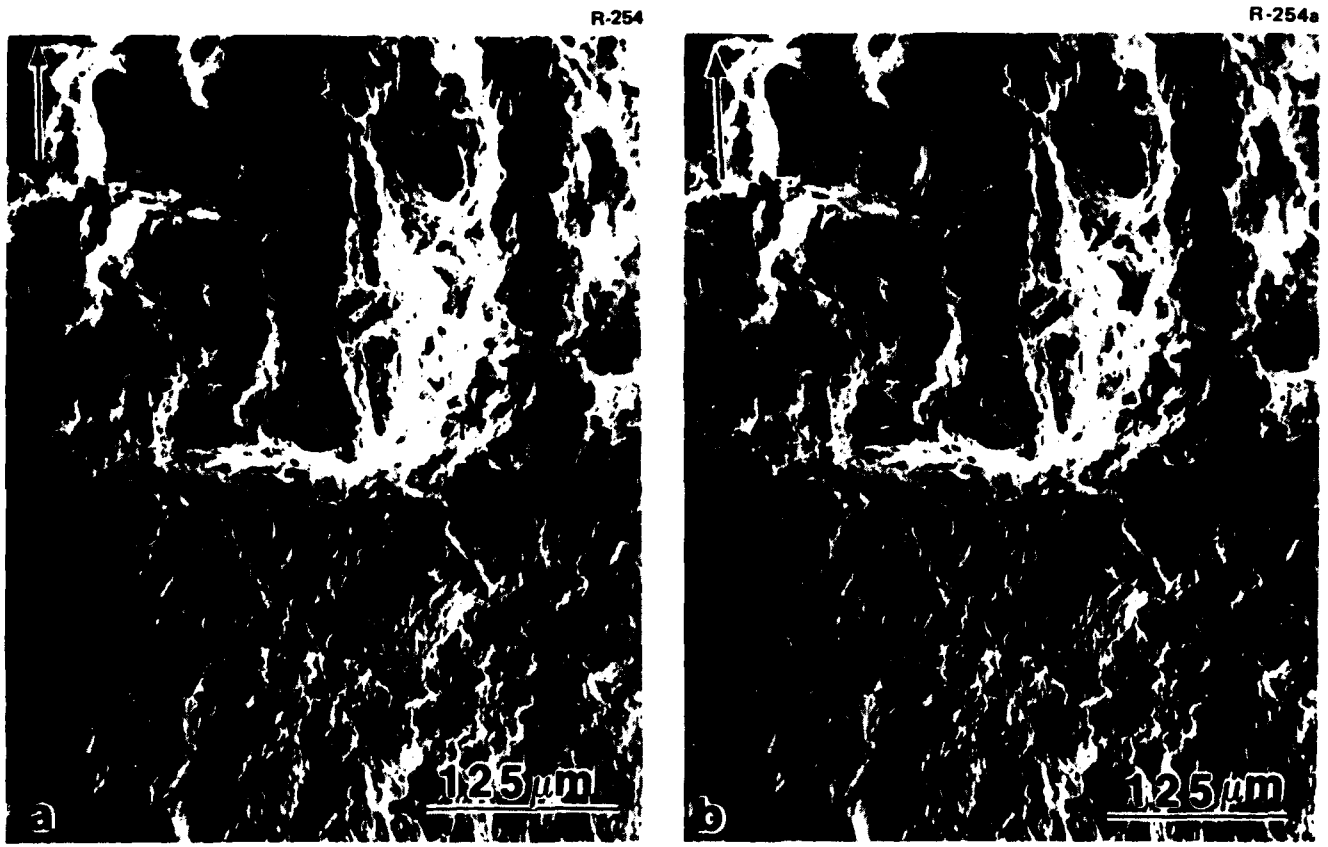

Fig. 12 — Stereo pair of SEM fractograph of Alloy HT-9, Heat 91354, tested at 24°C. Arrows show direction of macroscopic crack propagation. This stereo pair was used to generate crack profile shown in Fig. 13.

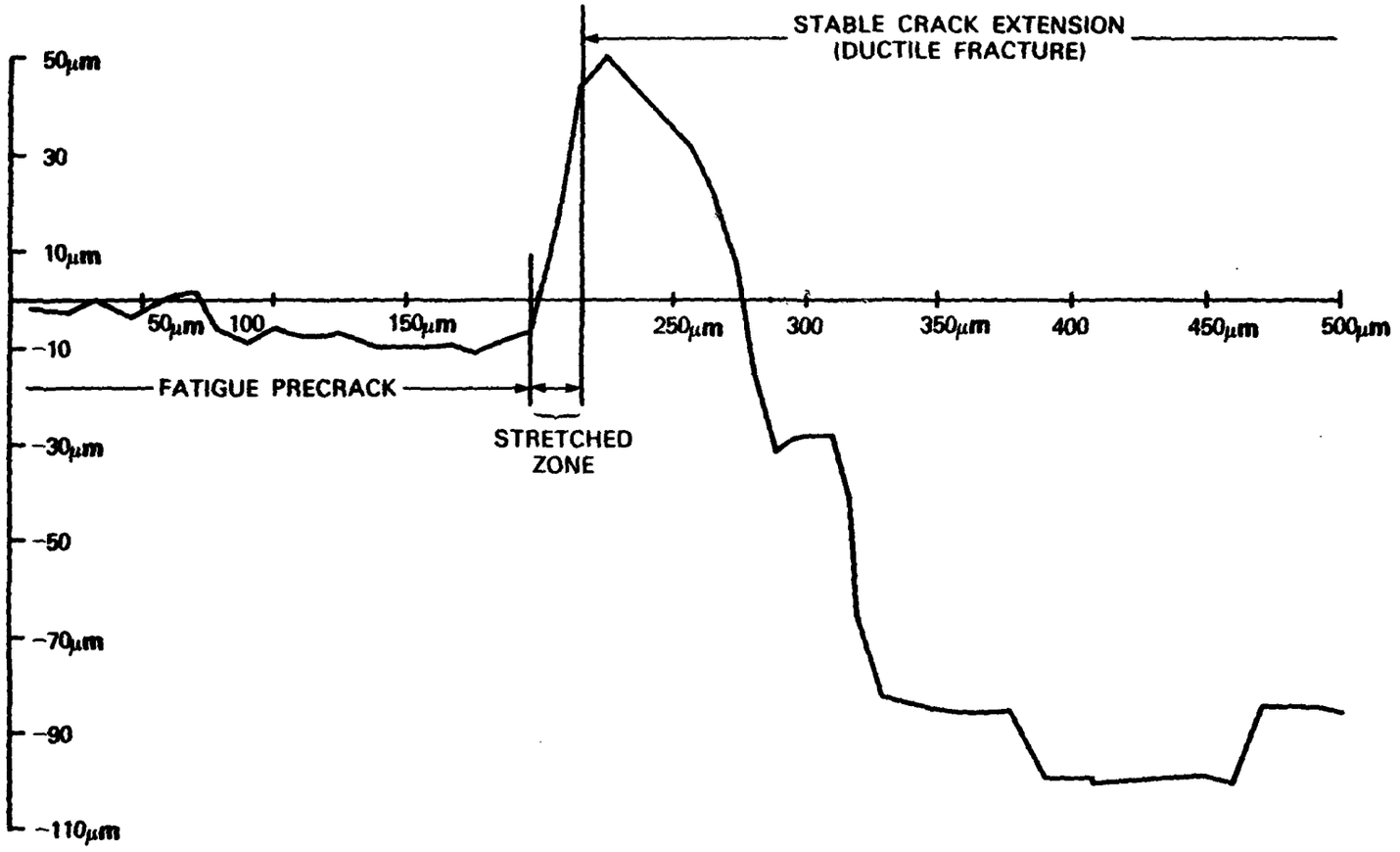

Fig. 13 — Typical crack profile used to measure the size of the stretched zone and the depth of large voids in the fracture surfaces of the CT specimens.

The SEM micrographs shown in Fig. 14 summarize the significant fractographic observations of the 2.5 mm specimen tested at 24°C. Figure 14a shows a large shear lip, indicative of gross plastic deformation. The higher magnification SEM stereo pair shows the following important features: (1) the crack front of the thinner specimen was very irregular; (2) the fracture surface in this specimen had a large shear component; (3) the crack extension region had primarily small microvoids; and (4) contrary to the case of the thicker specimens, the stretched zone in the thin specimen was small and poorly defined. The lack of clear definition of the stretched zone together with the pronounced irregularity in the crack front made it quite difficult to measure the average SZ in the 2.5 mm specimen. The other 2.5 mm thick specimen tested at 200°C revealed fracture features similar to those observed on specimens tested at 24°C. This can be seen from the SEM micrographs presented in Fig. 15.

Table 1 is a summary of the SZ measurements performed both on the 12.7 and 2.5 mm thick specimens. The COD at fracture initiation was taken to be two times the average stretched zone size. The validity of this assumption was checked by conducting stereographic measurements on the mating fracture surfaces. The crack initiation at fracture occurred roughly in the middle of the stretch zone.

TABLE 1 - Summary of J-Integral Values, Corresponding Stretched Zone Height, and Constraint Factor for HT-9 Alloy Tested at 24 and 200°C

	J_{Ic} in kj/m^2	Flow Stress in MPa	Stretched Zone Height in μm	COD-Value in μm	Constraint Factor-m
HT-9 - 1 0.5T at 24°C	110	738	38	76	2.0
HT-9 - 2 0.5T at 200°C	131	660	48	96	2.1
HT-9 - 1 0.1T at 24°C	170	738	19	38	6.1
HT-9 - 2 0.1T at 200°C	186	660	23	46	6.1

DISCUSSION

The results of the J tests showed that the value of J necessary to initiate stable crack extension from the 2.5 mm thick specimens was larger than the value for the 12.7 mm specimens. A criterion for the validity of J testing is being considered by the ASTM E24 Committee; a possible standard is that [17]:

$$B \geq 25 \frac{J_Q}{y} \text{ and} \tag{10}$$

$$b \geq 25 \frac{J_Q}{y} \tag{11}$$

where J_Q is the unvalidated value of J necessary to initiate stable crack extension, J_{Ic}

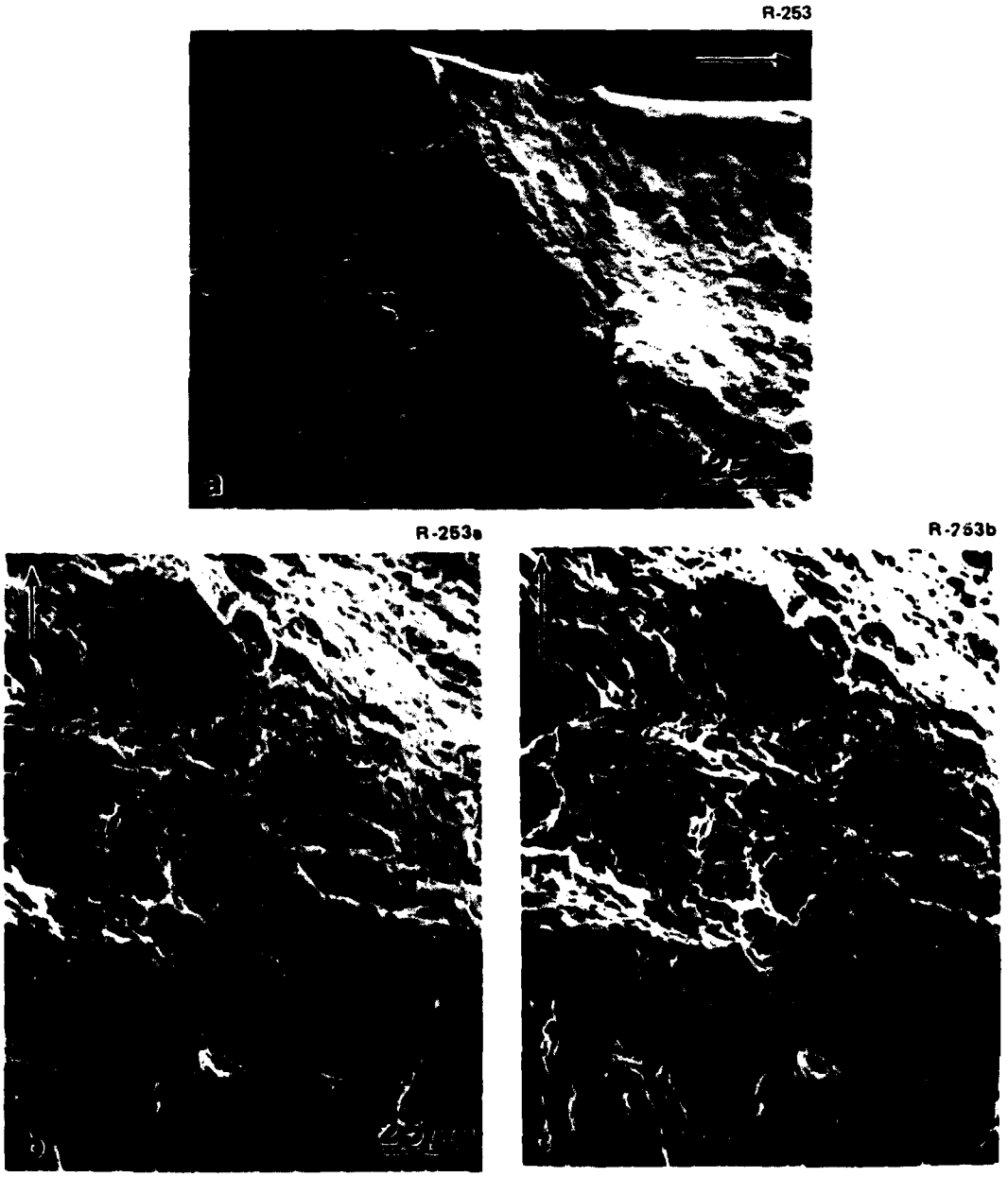

Fig. 14 — Figure surfaces (SEM) of 0.1T-CT specimen of Alloy HT-9, Heat 91354, tested at 24°C. Arrows show direction of macroscopic crack propagation. The micrographs show that in the thin specimen, the crack front is very irregular, the stretched zone is ill defined, and extensive plastic deformation occurred in the specimen bulk.

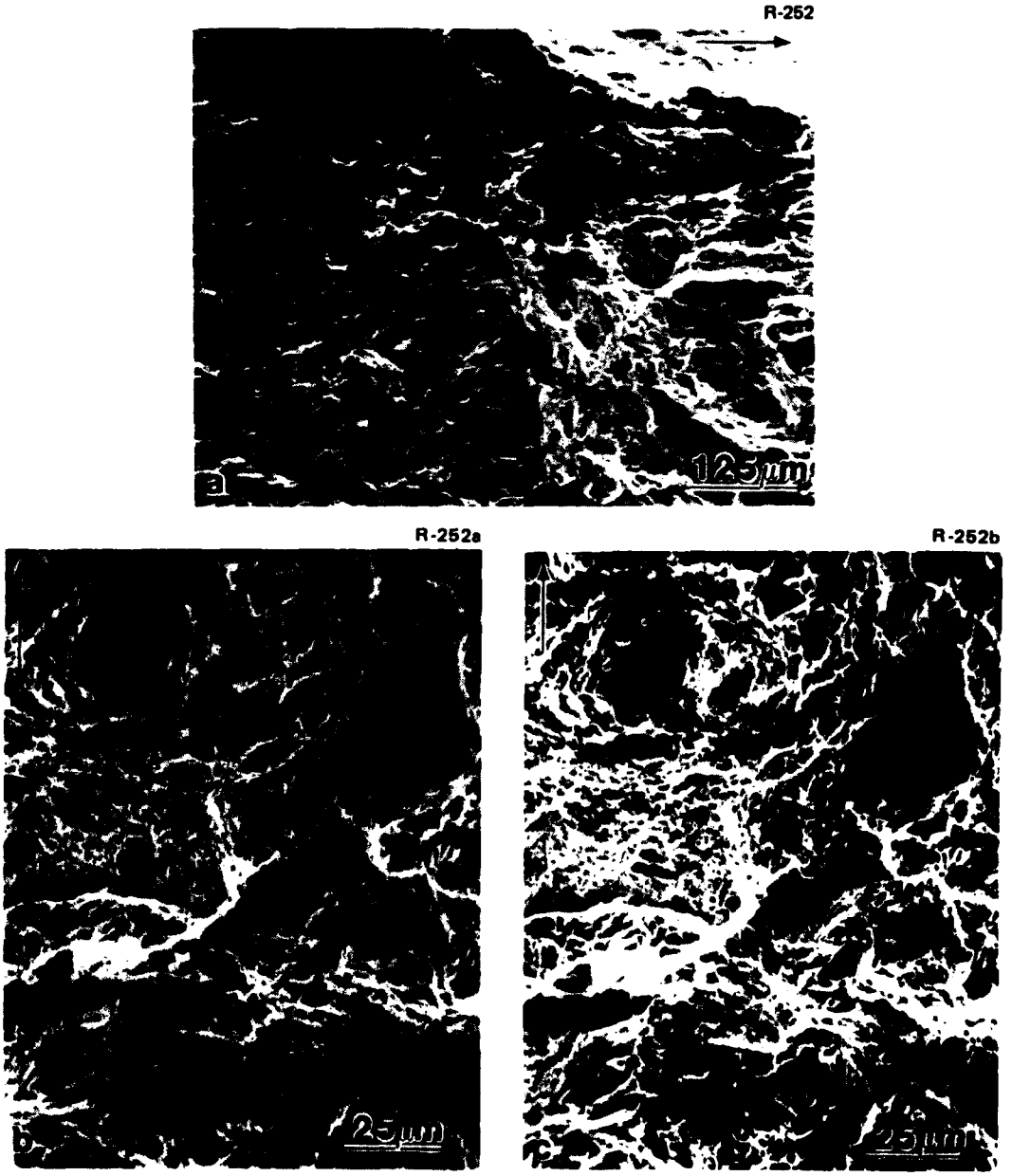

Fig. 15 — Fracture surfaces (SEM) of 0.1T-CT specimen of Alloy HT-9, Heat 91354, tested at 200°C. Arrows show direction of macroscopic crack propagation. The micrographs show that the main fractographic features present in this specimen are very similar to the features observed in the thin specimen tested at lower temperature.

is a valid value of J_Q, B is the thickness, and b is the initial unbroken ligament size. Taking J_Q to be 170 kJ/m^2 the critical dimension is 6.4 mm. The unbroken ligament dimension was nearly twice this amount in all specimens, but the thickness of the 2.5 mm specimens was less than half of the critical dimension. The 2.5 mm thick specimens would not satisfy the validity criteria being considered by the ASTM E24 Committee. The thinness of this specimen had considerable effect on the experimental results as discussed below.

The best correlation between fracture surface microstructure and J_{Ic} was obtained from the magnitude of the stretched zone in the 12.7 mm thick specimens. The value of the factor m was approximately 2.0 at both 24 and 200°C. The factor of 2.0 is smaller than the 2.25 factor observed by Broek for aluminum alloys; however, the factor of 2.0 is in reasonable agreement with the range of values from about 1 to 3 observed in the literature. Thus, we conclude that the magnitude of the stretched zone in the 12.7 mm thick specimens was a reasonable measure of J_{Ic}.

The 2.5 mm thick specimens did not yield a reasonable correlation between the stretched zone and J_Q. The stretched zone in the 2.5 mm specimens was not well defined, but where a stretched zone could be identified, it was significantly smaller than in the 12.7 mm specimens. A constraint factor (m) of about 6 was obtained for these specimens. This cannot be considered as a reasonable result because the constraint in the thin specimen should be less than in the thicker specimen. A similar result for m in 2.5 mm specimens has been observed by Gelles, et al [18].

The reason that equations of type 7 and 8 did not result in reasonable results for the thin specimen is that these equations have an inherent assumption that the plastic deformation is confined to a narrow band along the plane of the crack as was pointed out by Burdekin and Stone [2]. In the 2.5 mm specimens the plastic deformation extended through the volume of the material, thus the extension to out of plane deformation in the 2.5 mm specimens violated a basic assumption in the derivation of the equations relating J_{Ic} to COD.

The small size of the stretched zone in the 2.5 mm specimens was not in agreement with the magnitude of the load displacement. For the specimens tested at 24°C the load displacement was 0.046 cm in the 12.7 mm specimen and 0.076 cm in the 2.5 mm specimen. If the crack faces are assumed to be straight from a hinge point, then the ratio of the crack opening displacements should be equal to the ratio of the load line displacements. The 2.5 mm specimen has the larger load line displacement but a smaller crack opening displacement as measured by the size of the stretched zone. Thus the displacemment at the stretched zone does not reflect the full displacement at the load line. The other component of displacement that occurred at the load line, but not in the stretched zone, was plastic deformation in the bulk of the specimen. In the 12.7 mm specimen the plastic deformation was concentrated in the fracture plane, but in the 2.5 mm thick specimen the plastic deformation extended from the fracture plane to the bulk of the specimen. The larger load line displacement present in the 2.5 mm specimens appears to be reasonable because of through thickness plastic deformation. However, it is still difficult to explain why the stretched zone was smaller in the 2.5 mm specimens than in the 12.7 mm specimens.

The observation that the stretched zone height and the amount of shear lip was different in the 2.5 mm specimens than in the 12.7 mm specimens has implications

concerning the use of 2.5 mm specimens for fracture toughness determination. The fracture toughness of the 2.5 mm specimens was significantly higher than the 12.7 mm specimens; the higher fracture toughness was most likely due to plastic deformation out of the plane of fracture in the 2.5 mm specimens. Since the fracture microprocesses are different in the thick and in the thin specimens, it is possible that fracture in the thick and thin specimens would have different response to changes in environment. In these tests the value of J_{Ic} in the thicker specimens exhibited a greater temperature dependence than the thinner specimens. By changing the temperature from 200°C to room temperature J_{Ic} in the 12.7 mm specimen dropped 20 percent, whereas J_Q in the 2.5 mm specimen dropped only 9 percent.

CONCLUSIONS

1. In specimens of 12.7 mm thickness the stretched zone height gave a reasonable measure of J_{Ic} when utilized with Eq. (7).

2. In thinner specimens of 2.5 mm width the stretched zone height did not give a reasonable measure of J_Q.

3. The values of J_Q from 2.5 mm specimens were higher and had less temperature dependence than J_{Ic} values from 12.7 mm thick specimens.

4. Out of plane deformation in the 2.5 mm specimen appears to be responsible for the differences observed relative to the 12.7 mm specimen, and this result supports the necessity of the validity criteria proposed by the ASTM Committee E24.

ACKNOWLEDGMENTS

This work was supported by the Office of Naval Research. The authors wish to express their appreciation to Dr. James Sprague for assistance with the stereographic measurements and to Dr. Frank Loss for helpful discussions.

REFERENCES

[1] A. A. Wells, Proceedings of the Symposium on Crack Propagation, Cranfield, Vol. 1, pp. 210-230 (1961).

[2] F. M. Burdekin and D. E. W. Stone, J. Strain Analysis, Vol. 1 (No. 2); pp. 145-153, (1966).

[3] D. S. Dugdale, J. Mech. Phys. Solids, Vol. 8 (No. 2): pp. 100-104 (1960).

[4] D. Broek, Engineering Fracture Mechanics, Vol. 6: pp. 173-181 (1974).

[5] J. R. Rice, Trans. ASME, Series E, J. Appl. Mech., pp. 379-386 (1968).

[6] J. A. Begley and J. D. Landes, in Fracture Toughness, ASTM STP 514 (1972), a. 1-23 b. 24-39.

[7] J. F. Knott, Metal Science, Vol. 14:No. 8 & 9:pp.327-336 (1980).

[8] H. Kobayashi, H. Nakamura, K. Hirano and H. Nakazawa, "The J-Integral Evaluation of the Crack Tip Plastic Blunting and the Elastic-Plastic Fracture," Proceedings of US-Japan Joint Seminar on Fracture Mechanics and Its Application to Energy Related Structures, Hayama, Japan, 12-16 Nov 1979.

[9] B. A. Fields and K. J. Miller, Engineering Fracture Mechanics, Vol. 9:pp. 137-146 (1977).

[10] J. R. Rice and M. A. Johnson, pp. 641-672 in Inelastic Behaviour of Solids, M. F. Kanninen. W. F. Adler, A. R. Rosenfield and R. I. Jaffee (Eds.), New York, McGraw-Hill (1970).

[11] J. D. Landes and D. E. McCabe, "Proceedings of the Third International Conference on Materials," Vol. 3: pp. 539-547 (1979), Cambridge, England.

[12] F. J. Loss (Ed.), "Structural Integrity of Water Reactor Pressure Boundary Components, QPR, Apr-Jun 1979," NUREG/CR-0943, NRL Memorandum Report 4064, Naval Rsearch Laboratory, Sep 28, 1979.

[13] J. R. Hawthorne (Ed.), "The NRL-EPRI Research Program (RP886-2), Evaluation and Prediction of Neutron Embrittlement in Reactor Pressure Vessel Materials, Annual Progress Report for CY 1978," NRL Report 8327, Naval Research Laboratory, Aug 30, 1979.

[14] J. A. Sprague, "Automated Data Reduction from Transmission Electron Micrographs," AIME Symposium on Advanced Techniques for the Characterization of Microstructures, Las Vegas, NV, 25-28 Feb 1980.

[15] L. E.Thomas, "Quantitative Stereoscopy in the HVEM," pp. 460-461 in Proceedings of the Thirtieth Annual Meeting of the Electron Microscopy Society of America, G. W. Bailey, Ed., Claitor's Publishing Division, Baton Rouge, LA (1972).

[16] F. A. Smidt, Jr., J. R. Hawthorne, and V. Provenzano, "The Fracture Resistance of HT-9 After Irradiation at Elevated Temperature," pp. 269-283 in Proceedings of the Symposium on Effects of Radiation on Structural Materials, ASTM STP 725 (1981).

[17] "The Determination of the Elastic-Plastic Toughness Parameter, J_{Ic}," ASTM Committee E24.08.04, ASTM, Philadelphia, March 12, 1979.

[18] Private communication with D. S. Gelles.